Biochemical Pharmacology 175 (2020) 113908

Contents lists available at ScienceDirect

Biochemical Pharmacology

journal homepage: www.elsevier.com/locate/biochempharm

Novel indole derivatives targeting HuR-mRNA complex to counteract high glucose damage in retinal endothelial cells

Chiara Bianca Maria Platania[a], Valeria Pittalà[b], Alessia Pascale[c], Nicoletta Marchesi[c], Carmelina Daniela Anfuso[a,d], Gabriella Lupo[a,d], Martina Cristaldi[a], Melania Olivieri[a], Francesca Lazzara[a], Luisa Di Paola[e], Filippo Drago[a,d], Claudio Bucolo[a,d,*]

[a] Department of Biomedical and Biotechnological Sciences, School of Medicine, University of Catania, Catania, Italy
[b] Departement of Drug Sciences, University of Catania, Catania, Italy
[c] Department of Drug Sciences, Pharmacology Section, University of Pavia, Pavia, Italy
[d] Center for Research in Ocular Pharmacology-CERFO, University of Catania, Catania, Italy
[e] Unit of Chemical-Physics Fundamentals in Chemical Engineering, Department of Engineering, Campus Bio-Medico University, Roma, Italy

ARTICLE INFO

Keywords:
HuR
Diabetic retinopathy
VEGF
TNFα
Angiogenesis

ABSTRACT

The ELAVL1 (or human antigen R - HuR) RNA binding protein stabilizes the mRNA, with an AU-rich element, of several genes such as growth factors (i.e. VEGF) and inflammatory cytokines (i.e. TNFα). We hereby carried out a virtual screening campaign in order to identify and test novel HuR-mRNA disruptors. Best-scored compounds were tested in an *in-vitro* model of diabetic retinopathy, namely human retinal endothelial cells (HRECs) challenged with high-glucose levels (25 mM). HuR, VEGF and TNFα protein contents were evaluated by western-blot analysis in total cell lysates. VEGF and TNFα released from HRECs were measured in cell medium by ELISA. We found that two derivatives bearing indole moiety, VP12/14 and VP12/110, modulated HuR expression and decreased VEGF and TNF-α release by HREC exposed to high glucose (HG) levels. VP12/14 and VP12/110 inhibited VEGF and TNF-α release in HRECs challenged with high glucose levels, similarly to dihydrotanshinone (DHTS), a small molecule known to interfere with HuR- TNFα mRNA binding. The present findings demonstrated that VP12/14 and VP12/110 are innovative molecules with anti-inflammatory and anti-angiogenic properties, suggesting their potential use as novel candidates for treatment of diabetic retinopathy.

1. Introduction

Diabetic retinopathy (DR), a common complication of both type 1 and type 2 diabetes, is one of the leading causes of irreversible vision loss. Diabetic retinopathy is a disease with multifactorial etiopathogenesis, which include oxidative [1] and hypoxic [2] stress, inflammation [3], angiogenesis [4] as response of several cell type to hyperglycemia. To date, the approved pharmacological treatments (intravitreal steroids or anti-VEGF agents) target the late stage of the disease, namely proliferative diabetic retinopathy (PDR). These drugs aim at inhibiting inflammation and angiogenesis, the main etiopathogenetic processes leading to diabetic macular edema, which is, in turn, the major cause of retinal detachment and irreversible vision loss. Besides the impact and efficacy of anti-VEGF agents or steroids in the treatment of PDR, great interest has been raised by anti-TNFα intravitreal treatments (i.e. infliximab), although only one study, with a short follow-up, reported the beneficial effects of infliximab treatment in patients with diabetic macular edema [5,6]. Nevertheless, apart from the little clinical evidences about anti-TNF-α biologics, given that inflammation contributes significantly to the etiology and progression of diabetic retinopathy, a target therapy against TNFα is worthy of further investigation. We therefore explored in this study an alternative mechanism for TNFα and VEGF inhibition, by targeting the RNA binding protein ELAVL1 (or human antigen R, HuR). HuR is a chaperon protein able to bind transcripts encoding for several proteins, including some cytokines and growth factors. Therefore, HuR promotes the increase of cytoplasmic stability and/or rate of translation of the target mRNA, by preferentially interacting with adenine-uracil-rich elements (ARE), *cis*-acting elements localized within mRNA sequence [7]. The involvement of HuR in the stabilization of VEGF mRNA in DR has been previously demonstrated [8], and HuR silencing through intravitreal injection of siRNA nanoparticles prevented both HuR and VEGF overexpression in

* Corresponding author at: Department of Biomedical and Biotechnological Sciences, School of Medicine, University of Catania, Via Santa Sofia 97, 95125 Catania, Italy.
E-mail address: claudio.bucolo@unict.it (C. Bucolo).

https://doi.org/10.1016/j.bcp.2020.113908
Received 3 December 2019; Accepted 9 March 2020

diabetic rat retina [9]. Furthermore, HuR-siRNA nanoparticles preserved rat retinal structure from damage induced by diabetes [9]. Moreover, HuR binds and stabilizes TNFα mRNA [10], therefore HuR inhibition could be an alternative anti-inflammatory strategy.

The role of HuR in inflammation and other diseases boosted the interest towards the discovery of new inhibitors. However, only a restricted number of compounds have been identified so far as HuR inhibitors (agents that can prevent the formation HuR–RNA complex) [11–14]. Moreover, very few examples of *de novo* design, synthesis, and structure–activity relationships (SAR) studies of compounds interfering with HuR-mRNA interaction have been described to date [15,16]. Molecular modeling and structural studies have identified the active site of small HuR inhibitors in the pocket where the mRNA strand is bound. Therefore, we aimed to identify new HuR inhibitors by a validated virtual screening approach. A focused set (28 novel compounds) was selected on the basis compounds shape similarity to dihydrotanshinone (DHTS), starting from a proprietary compound database containing 182 ligands. Dihydrotanshinone (DHTS), a validated HuR inhibitor [10], served as a positive control both in the in-silico and in-vitro approaches. Structure–activity relationship studies around the chemotype of DHTS were not carried out due to structural complexity of this natural compound, indeed, we searched for simpler analogues, sharing shape and pose similarity with DHTS and other HuR inhibitors. The focused set of compounds was docked in the active cleft of HuR (PDB:4EGL) and the HuR-mRNA complex (PDB:4ED5) [17]. We identified two hit compounds with best docking score, VP12/14 and VP12/110, bearing an indole scaffold linked to a phenethyl ring through an ester or an acrylate function. These compounds were tested in an in-vitro model of diabetic retinopathy as potential HuR inhibitors, endowed with anti-angiogenic and anti-inflammatory properties. For this purpose, human retinal endothelial cells (HRECs), challenged with high glucose levels (25 mM), were treated with VP12/14 and VP12/110, and then HuR, VEGF-A and TNF-α levels have been assessed. Molecular dynamics simulations of HuR-inhibitors and HuR-mRNA-inhibitors gave some indications of the mechanism of action of the tested compounds, endowed with anti-angiogenic and anti-inflammatory activity in *in vitro* model of diabetic retinopathy.

2. Material & methods

2.1. Protein contact network analysis

In order to predict, with an unbiased method, the binding pocket of HuR inhibitors, we carried out a protein contact network (PCN) analysis that identified allosteric residues in HuR. The structural information embedded into the PDB files (PDB: 4EGL apo structure of HuR; PDB: 4ED5 holo structure of HuR [17]) were the input files used to generate the Protein Contact Networks (PCNs), respectively for apo- and holo-structures. Network nodes were the HuR residues identified by their α–carbons. The edges between nodes (residues) were build, given for a couple of residues a cut-off of Euclidean distance equal to 4–8 Å, in order to account only for significant non-covalent intra-molecular interactions. The generic element adjacency A_{ij} of the adjacency matrix A was 1 if i-th and j-th nodes were connected by an edge, otherwise was 0. Starting from the matrix A it is possible to derive several descriptors defining the wiring architecture of PCNs. The simplest network descriptor is the node degree, defined for each node as the number of links it participates in. The shortest path between two nodes is defined as the minimum number of links connecting them. For a PCN it is possible to compute the shortest path SP matrix, in which the generic element sp_{ij} represents the number of links connecting the i-th and the j-th residues. The average value *asp* is the average value over all pairs of residues, it computes the efficiency in signal transmission within the network (lowest *asp* corresponds to best communication). Allosteric movements or properties in proteins have been linked to specific protein domain sites defined as modules [18]. Thus, it is crucial to identify modules in PCNs, that generally match with recognized protein functional domains [19]. We applied spectral clustering (a binary partition method) to identify functional modules in protein structures [20,21]. Based on the cluster partition, the participation coefficient P is calculated. The participation coefficient is able to identify key residues (nodes) for signal transmission throughout the protein. The variation of P (dP) upon binding was previously recognized as an indicator of allosteric response in proteins [21–23]. The dP is generally not due to displacement, as shown also in this work. The dP values have been mapped in protein structures and visualized as temperature scale by means of a python script previously implemented in Pymol [24].

2.2. Molecular modelling

Before virtual screening, we carried out model validation of structures used in the docking protocol. Training sets of known active and inactive compounds at HuR were docked both into 4EGL and 4ED5 structures. The active training set included: okicenone [25], quercetin [26], MS444 [25], dehydromutactin [25], B40 [26], B41 [26], and dihydrotanshinone I [10]. Inactive training sets included: Mutactin [25], AUR367 [25], B68 [26] and B63 [26]. The SiteMap task in Schrodinger©-Maestro served, along with PCN analysis, as an input of the Grid Generation task. Ligands of the training set, and docked ligands were converted from .sds file format to suitable format for Schrodinger Maestro by means of the LigPrep task, then assigning ligands ionization state at pH = 7.4. Molecular docking was carried out with the following protocol: (i) grid generation on the centroid of the binding pocket; (ii) standard precision (SP) docking (Schrodinger©) performed with Glide (Schrodinger©). At first, docking was carried out with ring conformation sampling, followed by a 500-step conjugate gradient minimization by Glide (dielectric = 1). MM-GBSA rescoring, of semiflexible docking poses at binding pockets of 4EGL and 4ED5 models, was carried out by means of Schrodinger© Maestro: the VSGB 2.0 model was used and all residues within 15 Å from the ligand were capable to move during the energy minimization with conjugate gradient algorithm. Active and inactive compounds were clustered on the basis energetic terms of predicted $\Delta G_{binding}$, which is the output of MM-GBSA calculations. Only active and inactive compounds significantly clustered based on computed $\Delta G_{coulomb}$ values. In order to further validate the virtual-screening and decrease the false-positive discovery rate, the explored focused compound dataset, after molecular docking, was analyzed and clustered by means of structural interaction fingerprints (SIFts) using the corresponding Maestro-Schrodinger© task. The focused set of screened ligands, 28 novel compounds, was generated from shape similarity analysis (DHTS as template, Canvas® Schrodinger) carried out on a proprietary dataset of 182 ligands, which included: pyrrolopyrimidindione, benziloxyindol, indole, long-chain arylpiperazines (LCAP), pyrimidinketodiazole, quinoline, thiophene and caffeic acid phenethyl ester (CAPE) derivatives [27–32]. Finally, only 28 compounds including indole and CAPE derivates were docked, along with indomethacin, CAPE, and the training sets (active and inactive compounds). Prediction of ADME properties of the tested compounds was carried out with the QikProp task of Schrodinger Maestro©, including the following steps: (i) ligands preparation with LigPrep task; (ii) launching of the QikProp task as previously described [33]. Predicted ADME properties included: CNS predicted activity (from −2, the worst, to 2 the best); human oral absorption (1 low, 2 medium, 3 high), number of metabolic reactions, rule of five (number of violations of Lipinski's rule of five), parameters indexing skin (QPlogKp, Jm) and brain (CNS, QPlogBB QPPMDCK) penetration ligand propensity. In order to deeply analyze, at the structural level, the mechanism of action of HuR inhibitors, we used Desmond (task of Schrodinger) to carry out molecular dynamics simulation of the following complexes: i. HuR-DHTS; ii. HuR-VP12/14; iii. HuR-VP12/110; iv. HuR-mRNA (4ED5); v. HuR-mRNA-DHTS; vi. HuR-mRNA-VP12/14; vii. HuR-mRNA-VP12/110. Simulated systems were built with the "System Builder" task of

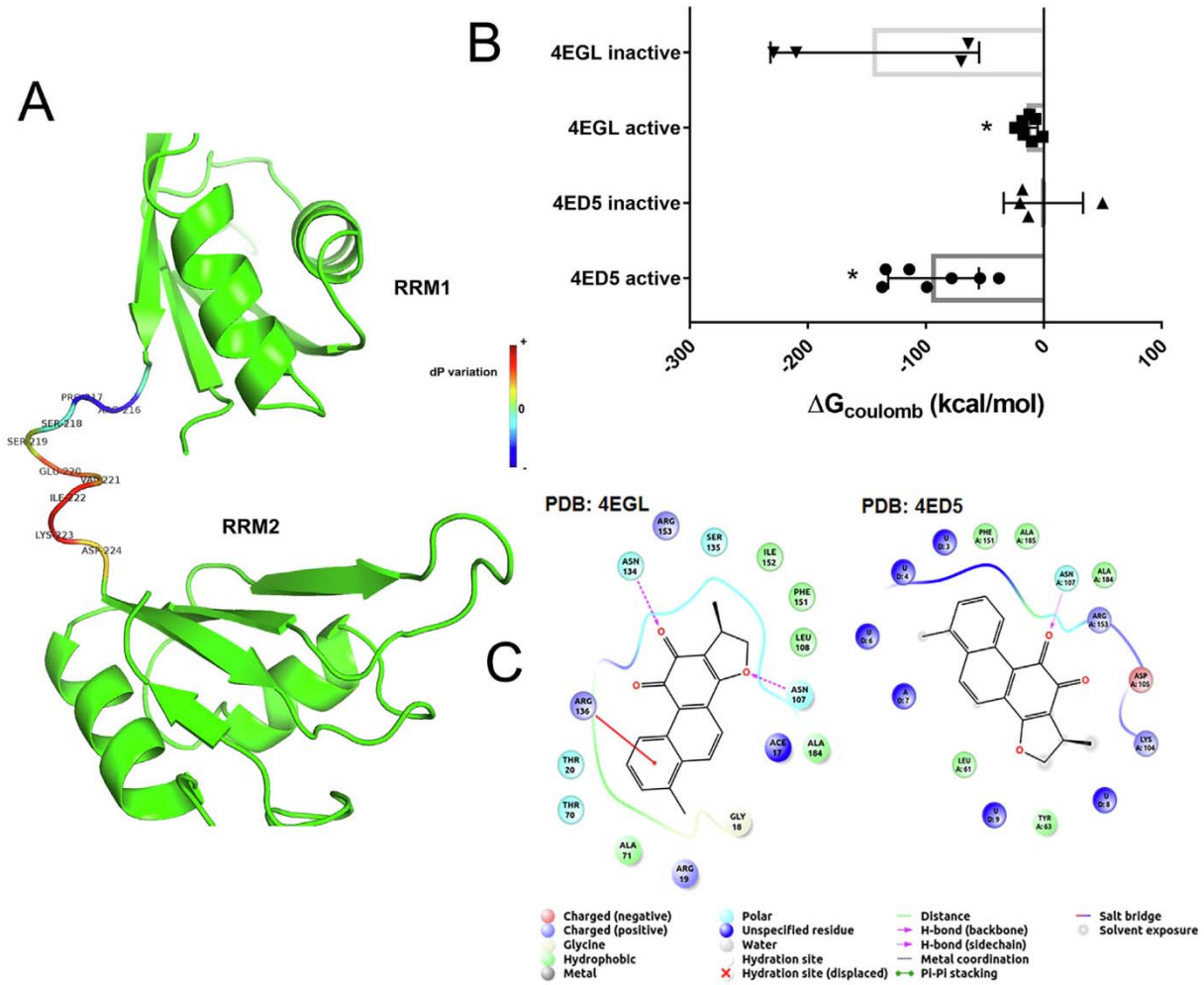

Fig. 1. Allosteric residues (high dP values from PCN analysis) belong to the RRM1-RRM2 connecting loop and validation of virtual screening protocol. A) Ribbon structure of the apo form of HuR, dP values were mapped (heat map color scale) in the structure of HuR. B) Active compounds showed statistically significant differences compared to inactive compounds docked on the apo (4EGL) and holo (4ED5) structure of HuR. C) 2D representation of pose of DHTS, a validated HuR inhibitor, bound to HuR models used for virtual screening.

Schrodinger® Maestro as follows: i. triclinic box with minimized overall volume and 15 Å dimension of z-coordinates; ii. OPLS parameters where assigned to protein-ligand; iii. The TP3P explicit water model was used and Na^+ Cl^- ions where added to neutralize the system at 150 mM final concentration. Before MD production (1.2 ns for each complex), the systems were subjected to automatic protein-in-water relaxation protocol. After relaxation steps, MD production runs were carried out as follows: (NPT) ensemble, Nosé-Hoover thermostat at 310 K and Martyna-Tobias-Klein barostat at 1.01325 bar pressure. Atomic coordinates were collected every 2.4 ps and energy calculated every 1.2 ps. HuR-inhibitor and HuR-mRNA interactions in each complex have been analyzed with the "Simulation Interaction Diagram" task of Schrodinger® Maestro.

2.3. Chemistry

Melting points were determined in an IA9200 Electrothermal apparatus equipped with a digital thermometer in glass capillary tubes. Infrared spectra were recorded on a Perkin Elmer 281 FTIR spectrometer in KBr disks or NaCl crystal windows. Elemental analyses for C, H, N, and S were within ± 0.4% of theoretical values and were performed on a Carlo Erba Elemental Analyzer Mod. 1108 apparatus. ^1H NMR spectra were recorded on Varian Inova Unity 200 (200 MHz) spectrometers in DMSO-d_6 solution. Chemical shifts are given in δ values (ppm), using tetramethylsilane as the internal standard; coupling constants (*J*) are given in Hz. Signal multiplicities are characterized as s (singlet), d (doublet), t (triplet), q (quartet), m (multiplet), br (broad signal). All the synthesized compounds were tested for purity with Thin Layer Chromatography (TLC, aluminum sheet coated with silica gel 60 F254, Merck) and visualized by UV (λ = 254 and 366 nm). Purification of synthesized compounds by flash column chromatography was performed using Biotage FlashMaster Personal plus with SNAP cartridges KP-SIL. All chemicals and solvents were reagent grade and were purchased from commercial vendors.

2.4. VP12/14 and VP12/110 synthesis

The appropriate starting carboxylic acid (2 mmol) was dissolved in 5 mL of DMSO. Exsiccated Na_2CO_3 (2.4 mmol) was added while stirring. The mixture was left stirring for 30 min, then a solution of the appropriate (2-bromoethyl) substituted-aryl (2.25 mmol) in 1 mL of DMSO was added over a period of 30 min. After that, a catalytic amount of potassium iodide was added, and the reaction mixture was left stirring at room temperature for 24 h. To the obtained suspension was added with 50 mL of a solution of $NaHCO_3$ 5%, and the aqueous layer was washed with ethyl acetate (3 × 50 mL). The combined organic layers were washed with brine (1 × 100 mL), dried over anhydrous Na_2SO_4, filtered, and evaporated.

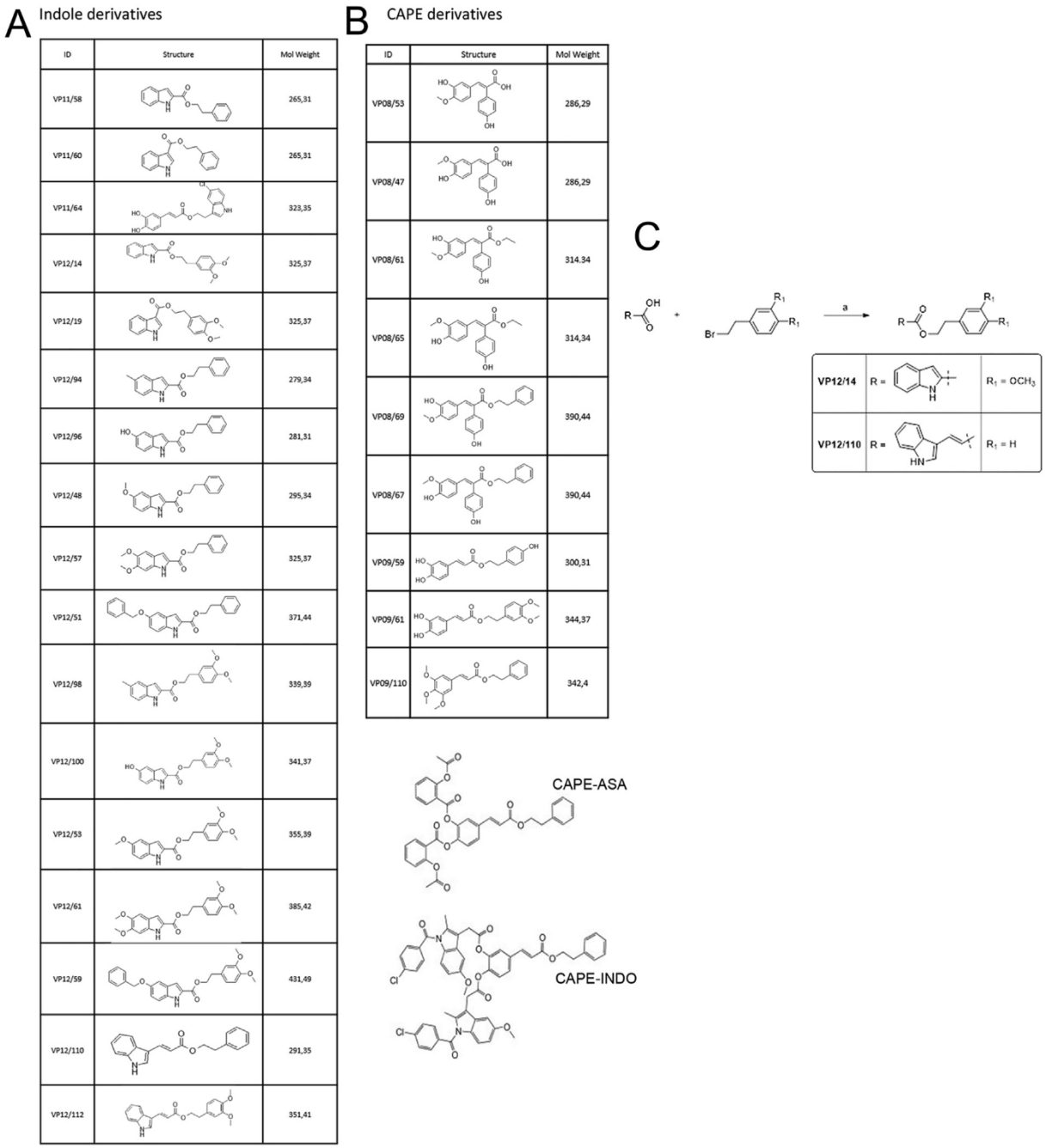

Fig. 2. Screened compounds and VP12/14 and VP12/110 chemical synthesis. A) Indole derivatives. B) Caffeic Acid Phenethyl Ester derivatives. C) synthesis: (a) Reagents and conditions: K_2CO_3, KI, DMSO, 22 °C, 22 h.

2.4.1. 1H-Indole-2-carboxylic acid 2-(3,4-dimethoxyphenyl)ethyl ester (VP12/14).

VP12/14 compound was isolated as a pure off-white solid (85%), mp 144–146 °C; IR (KBr) cm^{-1} 3315, 2946, 1699, 1518, 1462, 1398, 1314, 1253, 1206, 1156, 1026, 956, 753; ^1H NMR (DMSO-d_6): δ 11.91 (br s, 1H, NH), 7.73–7.62 (m, 1H, aromatic), 7.50–7.45 (m, 1H, aromatic), 7.32–7.20 (m, 1H, aromatic), 7.17–7.01 (s, 2H, aromatic), 6.98–6.78 (m, 3H, aromatic), 4.47 (t, J = 6.8 Hz, 2H, OCH_2CH_2), 2.98 (t, J = 6.8 Hz, 2H, OCH_2CH_2). Anal. Calcd. for $C_{19}H_{19}NO_4$: C, 70.14; H, 5.89; N, 4.30. Found: C, 70.47; H, 5.90; N, 4.25.

2.4.2. Phenethyl (E)-3-(1H-indol-3-yl)acrylate (VP12/110)

VP12/110 was isolated as a pure light orange solid (81%), mp 115–116 °C; IR (KBr) cm^{-1} 3242, 1677, 1613, 1576, 1440, 1273, 1229, 1181, 1120, 979, 744; ^1H NMR (DMSO-d_6): δ 11.81 (br s, 1H, NH), 7.99–7.77 (m, 3H, aromatic), 7.53–7.09 (m, 7H + 1H, aromatic + C*H* = CHCOO), 6.34 (d, J = 16 Hz, 1H, CH = C*H*COO) 4.34 (t, J = 6.8 Hz, 2H, OCH_2CH_2), 2.98 (t, J = 6.8 Hz, 2H, OCH_2CH_2). Anal. Calcd. for $C_{19}H_{17}NO_2$: C, 78.33; H, 5.88; N, 4.81. Found: C, 78.69; H, 5.88; N, 4.29.

2.5. Cell culture and cell viability

The primary human retinal endothelial cells (HRECs, cell passage #4–6) were purchased from Innoprot (Elexalde Derio, Spain) and cultured with ECM (endothelial cell medium) supplemented with 5% fetal bovine serum (FBS), 1% endothelial cell growth supplement (ECGS), 100 U/mL penicillin, and 100 mg/mL streptomycin. HRECs were grown

Table 1
Predicted $\Delta G_{coulomb}$ of screened compounds.

ID	4EGL ($\Delta G_{coulomb}$ Kcal/mol)	4ED5 ($\Delta G_{coulomb}$ Kcal/mol)
CAPE derivatives		
CAPE-ASA	−9	−113
CAPE-INDO	−20	−91
VP08/61	−5	−117
VP08/67	9	−90
VP09/119	−12	−64
VP08/53	−116	−9
VP08/65	−26	−76
VP09/61	0,96	−84
VP08/47	−89	−8
VP08/59	−32	−117
CAPE	−16	−84
Indole derivatives		
VP12/110	33	−88
VP12/14	63	−75
VP12/112	64	−64
VP11/64	56	−132
VP12/96	27	−84
VP12/61	37	−109
VP12/53	61	−136
VP12/48	44	−81
VP11/58	23	−102
VP12/94	26	−88
VP12/98	79	−87
VP12/57	31	−101
VP11/60	46	−94
VP12/51	48	−106
VP12/100	60	−88
VP12/19	69	−95
VP12/59	40	−60
VP11/60	43	−75
indomethacin	28	−46

at 37 °C, a humidified atmosphere of 5% CO_2. For all experiments, the cells were transferred to serum-starved medium with 1% FBS for 24 h. Viability of HRECs was evaluated with the MTT [3-(4,5-dimethylthiazol-2-yl)2,5-diphenyltetrazolium bromide] assay. At first, 1×10^4 HREC/well were seeded in a 96-well plate. HRECs were incubated with 25 mM of mannitol, this group served as osmotic control. Cells were also treated with DHTS (0.1–100 μM), VP12/14 (0.1–100 μM), VP12/110 (0.1–100 μM) in the presence or absence of high glucose levels (HG 25 mM) for 24 and 48 h. At the end of treatments, 15 μl of MTT (5 mg/ml) was added in each well for 3 h at 37 °C, 5% CO_2. Then 100 μl dimethyl sulfoxide (DMSO) was added to dissolve formazan crystals and absorbance was measured at 570 nm in a plate reader (Synergy 2-bioTek; Perkin Elmer, Waltham, MA, USA).

2.6. Western blotting analysis

The total protein content was measured via the Bradford's method, using bovine serum albumin as a standard. Proteins were diluted in 2X sodium dodecyl sulphate (SDS) protein gel loading solution, boiled for 5 min, separated on 12% SDS-polyacrylamide gel electrophoresis (SDS-PAGE) and processed following standard procedures. The mouse monoclonal anti- ELAV/HuR antibody (Santa Cruz Biotech, sc-5261 (3A2), lot: E0418) was diluted at 1:1000. The rabbit monoclonal antibodies were diluted as follows: the anti-VEGF (Abcam, Ab52917; lot: GR3219705-2) at 1:750 and the anti-TNFα (Santa Cruz Biotech, sc-133192 (C-4); lot: F0716) at 1:1000. The rat monoclonal antibody anti-α-tubulin (Thermo Scientific, MA1-80017, lot: 75269126) was diluted at 1:1000. The nitrocellulose membranes signals were detected by chemiluminescence and developed by ChemiDoc (Biorad). The optical density from the immunoblot of α-tubulin was used to normalize the data. Densitometric analysis was carried out by ImageJ 1.50i [34] (downloadable at http://imagej.nih.image/ij).

2.7. ELISA – VEGF-A, TNF-α measurements

VEGF-A and TNF-α were measured in culture medium using ELISA kits according to the manufacturer's instructions (#156–0001 from Enzo Life Sciences Inc. Farmingdale, NY, USA and #RAB0476 from Sigma-Aldrich St. Louis, MO, USA, respectively). In particular, the medium was harvested after 48 h of incubation with 25 mM mannitol, HG 25 mM, DHTS, (0.01–1 μM) VP12/14 and VP12/110 (0.1–10 μM). All experiments were performed in quadruplicates.

2.8. VEGFA qPCR and tube-formation assay

HRECs (cell passage # 4–6) were seeded in 60 mm Petri dishes ($2x10^5$) and grown in 5% fetal bovine serum (FBS), 1% endothelial cell growth supplement (ECGS), 100 U/mL penicillin, and 100 mg/mL streptomycin. The cells were shifted to serum-starved medium with 1% FBS for 24 h. Therefore, the following groups of cells were treated for 48 h with: 5 mM glucose medium (control); 25 mM glucose medium (HG); 25 mM glucose medium + DHTS (1 μM); 25 mM glucose medium + VP12/14 (10 μM); 25 mM glucose medium + VP12/110 (10 μM). Concentration of compounds was chosen on the basis of ELISA results. MIQE guidelines were followed in the present study. Extraction of total RNA, from HRECs, was done with TRIzol Reagent extraction method (Invitrogen, Life Technologies, Carlsbad, USA). The A_{260}/A_{280} ratio of the optical density of RNA samples in agarose gel electrophoresis blots (measured with Multimode Reader Flash, Varioskan™) was 1.95–2.01, in order to assess RNA purity. Retrotranscription was synthesized from 2 μg RNA with a reverse transcription kit (SuperScript™ II Reverse Transcriptase, Invitrogen, ThermoFisher Scientific, Carlsbad, USA). Real-time q-PCR was carried out with the LightCycler ® 2.0 (Real-Time PCR System Roche Life Science). The amplification reaction mix included iTaq™ Universal SYBR® Green Supermix (Biorad, Hercules, USA) and 1 μl (100 ng) of cDNA. Forty-five amplification cycles were carried out for each sample. Results were analyzed with the $2^{-\Delta\Delta}$Ct method. VEGFA (Forward 5′-GAGGTTTGAT CCGCATAATCTG-3′, Reverse 5′-ATCTTCAAGCCATCCTGTGTGC- 3′) expression was normalized to 18S mRNA levels (Forward 5′-AGTCCC TGCCCTTTGTACACA-3′; Reverse 5′-GATCCGAGGGCCTCACTAAAC-3′).

In order to confirm the anti-angiogenic activity of tested molecules (DHTS, VP12/14, VP12/110), tube-formation assay using Matrigel was carried out. HREC (cell passage #2–4; 1.5×10^4 cells/well) were seeded into pre-coated Matrigel (BD, Franklin Lakes, NJ) 96-well plate. The following experimental groups were included in the assay: 5 mM medium (control), 40 ng/ml VEGFA w/o DHTS (0.1–1 μM) VP12/14 (1, 10 μM), VP12/110 (1, 10 μM). The 96-well plate was incubated for 4 h at 37 °C, 5% CO_2, 95% humidity. Images were collected with a phase-contrast microscope at 4X magnification. Total tube length and the number of branch points of total neo-vessel network were measured with *ImageJ Software* [34].

2.9. Statistical analysis and graph design

Each experiment was carried out four times ($n = 4$) i.e. MTT, WB, ELISA, tube-formation assay and qPCR of VEGFA. Each experimental group was triplicated in each cell culture plate, petri dish or flask. Cell treatment and analysis was carried out by investigators who were unaware of group labels. After statistical analysis, labels were revealed by other two investigators, that designed the graphs. One-Way ANOVA test, followed by Tukey-Kramer *post hoc* test for multiple comparisons, were carried out. Differences between groups were considered significant for $p < 0.05$. Statistical analysis and graph design were carried out by means of GraphPad Prism 5 software (GraphPad Inc., San Diego, CA).

/

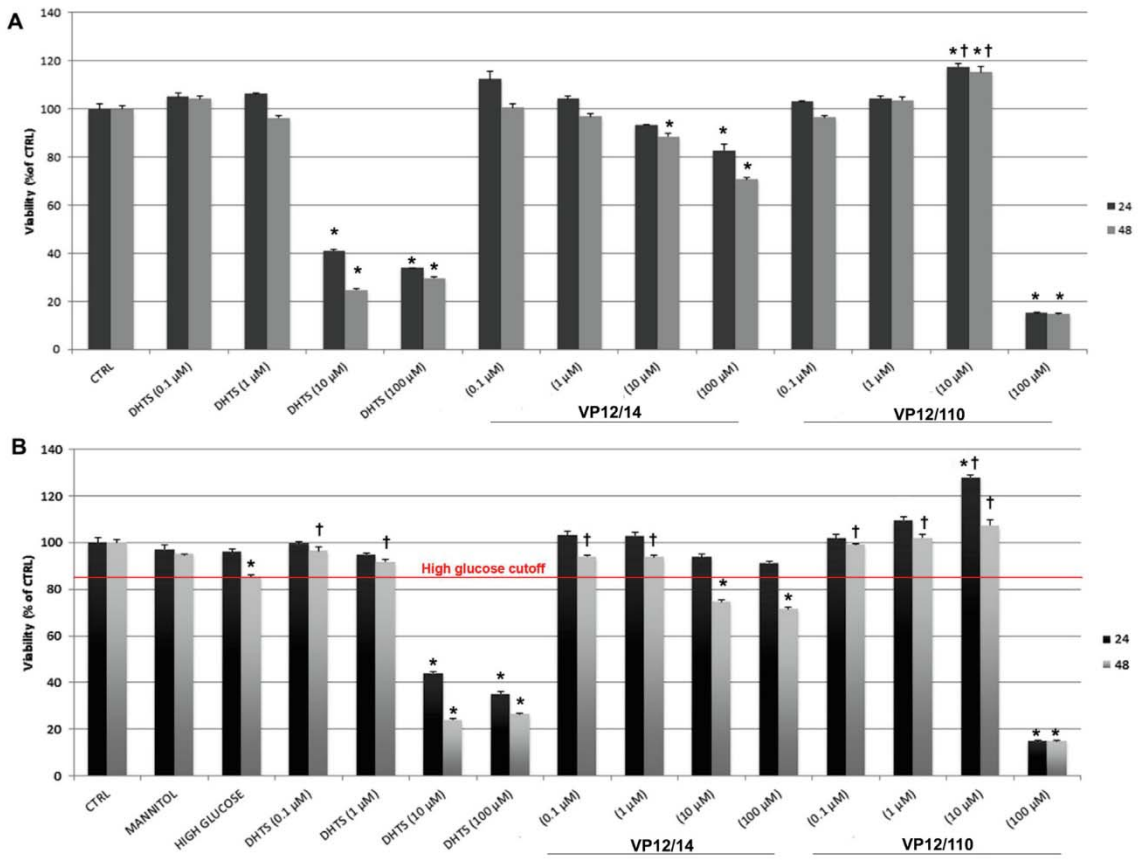

Fig. 3. MTT assay on HREC treated with DHTS, VP12/14 and VP12/110. HRECs were cultured, for 24 and 48 h, in a medium containing physiological glucose concentration (5 mM; CTRL, panel A) or high glucose levels (25 mM; high glucose, panel B) in the presence of different concentrations (0.1–100 μM) of DHTS, VP12/14 and VP12/110. The results are expressed as mean ± SD. Data were analyzed by one-way ANOVA, and Tukey post-hoc test for multiple comparisons. *p < 0.05 *vs* ctrl and † p < 0.05 *vs*. 1 μM DHTS (panel A) or high glucose (HG) group (panel B) (n = 4).

Table 2
Predicted ADME properties of DHTS, VP12/14 and VP12/110. #rtvFG number of reactive functional groups (predictive of decomposition or toxicity *in-vivo*). CNS predicted central nervous system activity on a –2 (inactive) to +2 (active) scale. QPlogBB, predicted brain/blood partition coefficient (orally delivered drugs) (−3 to 1.2); polar compounds, such as serotonine, cannot cross the blood-brain barrier (BBB) and have a more negative QPlogBB. #metab, number of predicted metabolites, predictive of *in-vivo* toxicity. QPPMDCK, predicted apparent MDCK cell permeability in nm/sec (> 500 great), MDCK (Madin-Darby Canine Kidney) cells are considered to be a good mimic for the BBB. QPlogKhsa, binding to human serum albumin (−1.5 to 1.5). Human oral absorption, predicted qualitative human oral absorption: 1 (low), 2 (medium), or 3 (high). Rule-Of-Five, number of violation (max 4) of drug-likeliness Lipinski's rules. Rule-Of-Three, number of violations (max 3) of Jorgensen's rule of three, likeliness of good oral bioavailability.

Molecule	#rtvFG	CNS	QPlogBB	QPPMDCK	#metab	QPlogKhsa	Human Oral Absorption	RuleOfFive	RuleOfThree
DHTS	2	0	−0,184	811,354	2	−0,089	3	0	0
VP12/14	0	0	−0,632	934,195	3	0,684	3	0	1
VP12/110	1	−1	−0,732	729,355	1	0,802	3	0	1

3. Results

3.1. In-silico identification of indole derivatives as HuR-inhibitors

The PDB: 4EGL and PDB: 4ED5 are the apo and holo structures, respectively, of the two N-terminals RNA-recognition motif (RRM) 1 and 2 of HuR. In particular, the PDB: 4ED5 is the X-ray structure of RRM1-RRM2 of HuR bound to the 11-base segment (5′-AUUUUUAU UUU-3′) of *c-fos* mRNA.

The two tandem RRM1 and RRM2 domains are linked by an nine residues long loop Arg216-Pro217-Ser218-Ser219-Glu220-Val221-Ile222-Lys223-Asp224 (Fig. 1A). This loop based on PNC calculations, was characterized by the highest absolute variations of participation coefficient (dP). High dP values identify the residues of HuR deputed to be allosteric residues, important for protein function (Fig. 1A). Molecular docking of training sets of active and inactive compounds at apo and holo structures of HuR was carried out, before MM-GBSA rescoring. Active and inactive compounds of the training sets significantly ($p < 0.05$) clustered together on the basis of differences in the electrostatic term ($\Delta G_{coulomb}$) of $\Delta G_{binding}$. Active compounds docked at 4EGL structure showed significant less negative $\Delta G_{coulomb}$ compared to inactive compounds (Fig. 1B). On the contrary, active compounds docked at 4ED5 structure were predicted to have more negative $\Delta G_{coulomb}$ compared to inactive compounds (Fig. 1B). Based on previous structural and functional studies on HuR inhibitors, we chose DHTS (Fig. 1C) as positive control inhibitor for both *in silico* and *in vitro* studies. The focused set of screened ligands, 28 compounds (Fig. 2A and B), came out from shape similarity analysis (DHTS as template, Canvas® Schrodinger) on a proprietary dataset of 182 ligands. After docking, MMGBSA rescoring was carried out on the explored compound dataset. We found that all indole derivatives had positive $\Delta G_{coulomb}$ values (Table 1), similarly to active HuR inhibitors (Fig. 1B). Clustering

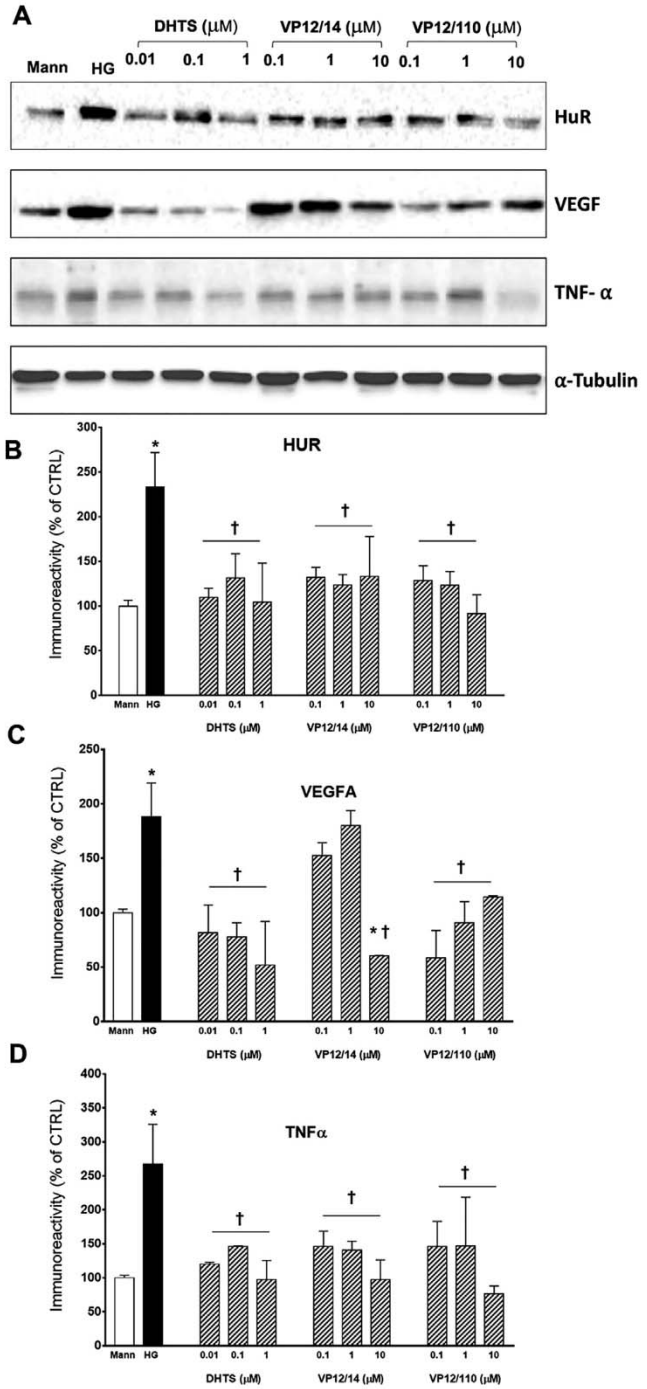

Fig. 4. Western blotting analysis of HREC total lysates for HuR, VEGFA and TNFα immunoreactivity. Representative blots (A). Densitometric analysis of HuR (B), VEGFA (C) and TNFα (D) immunoreactivities in the total homogenates of HRECs following exposure for 48 h to the osmotic control (mannitol; Mann) or high glucose levels (25 mM; HG) in the presence of different concentrations (0.01–1 μM) of DHTS, (0.1–10 μM) VP12/14 and VP12/110. The immunoreactivity of α-tubulin was used as a loading control. Results are expressed as % (± SD) with respect to the control HRECs (5 mM glucose). One-way ANOVA and Tukey *post-hoc* test for multiple comparison were carried out. *p $<$ 0.05 *vs.* Mann; † $<$ 0.05 *vs.* HG (n = 4).

analysis, by launching the Maestro structural interaction fingerprints (SIFts) task, guided the choice of hit compounds to be further tested *in vitro*. Only two compounds in the indole derivatives subset, VP12/14 and VP12/110, clustered in terms of SIFts and $\Delta G_{coulomb}$ with the active compounds DHTS and MS444 (SIFts ∩ MMGBSA $\Delta G_{coulomb}$ clustering). Other compounds of the active training dataset did not cluster (SIFts ∩ MMGBSA $\Delta G_{coulomb}$ clustering) with screened compounds.

3.2. Synthesis

The chemical synthesis of 1*H*-Indole-2-carboxylic acid 2-(3,4-dimethoxyphenyl)ethyl ester (VP12/14) and phenethyl (*E*)-3-(1*H*-indol-3-yl)acrylate (VP12/110) was achieved by coupling the corresponding starting material, 1*H*-indole-2-carboxylic acid or (*E*)-3-(1*H*-indol-3-yl) acrylic acid with 4-(2-bromoethyl)-1,2-dimethoxybenzene, or (2-bromoethyl)benzene, in DMSO and dry Na_2CO_3, at room temperature (Fig. 2C). The pure final products were easily obtained by flash chromatography purification using Biotage FlashMaster Personal plus. VP12/14 and VP12/110 were obtained with high yield ($>$ 80%) and were characterized by means of their ^{1}H NMR and IR spectroscopic data, melting points, and elemental analysis.

3.3. Safety profile of VP12/14 and VP12/110 on human retinal endothelial cells

Human retinal endothelial cells (HRECs) were grown in a medium containing physiological glucose concentration (ctrl, 5 mM) or high glucose levels (high glucose, HG, 25 mM) and were treated, for 24 and 48 h, with different concentrations (0.1–100 μM) of DHTS, VP12/14 and VP12/110 in order to assess any potential toxic effect of the tested compounds (MTT assay) (Fig. 3). DHTS, at 10 and 100 μM, decreased significantly cell viability of HRECs (CTRL and HG groups) both after 24 and 48 h of treatment. VP12/14 at 10 and 100 μM decreased HRECs (HG group) viability to 74.6 ± 0.4% and 71.5 ± 0.5%, respectively. While, VP12/110 did not significantly affect cell viability until tested at the 100 μM concentration (14.5 ± 0.3% of control) (Fig. 3A and 3B). Furthermore, VP12/110 (10 μM) increased significantly HRECs vitality (Fig. 3A and 3B). High glucose challenge (Fig. 3B) decreased HRECs viability only after 48 h exposure compared to control cells (5 mM glucose) or to osmotic control cells (25 mM mannitol). Based on these findings, we carried out further experiments on DHTS, VP12/14 and VP12/110 exposing the cells to drug concentrations lower than 100 μM. Prediction of ADME properties (Table 2) confirmed the potential higher toxicity (#number of reactive groups) of DHTS, compared to VP12/14 and VP12/110 in HRECs exposed to high glucose levels (HG). DHTS and VP12/14 were predicted to have a higher number of metabolites, 2 and 3 respectively, bearing a high predicted toxicity potential or off-target effects *in vitro* and *in vivo*, compared to VP12/110. ADME prediction showed that all the tested compounds had high drug-likeliness and good oral absorption. VP12/110, due to a lower apparent blood brain barrier permeability (QPPMDCK) and a slightly negative QPlogBB, was predicted to have a −1 CNS score (within the −2 (inactive) to +2 (active) score range).

3.4. VP12/14 and VP12/110 modulate HuR, VEGFA and TNFα protein expression in human retinal endothelial cells challenged with high glucose levels

High glucose challenge significantly ($p < 0.05$) increased the protein expression of HuR, VEGFA and TNFα (Fig. 4) in HRECs. DHTS, VP12/14 and VP12/110 treatments, at all the tested concentrations, significantly decreased HuR (Fig. 5A) and TNFα (Fig. 5C) expression in HRECs challenged with high glucose levels, although the effect was not concentration-dependent, possibly due to the typical low sensitivity of the western blotting technique. DHTS and VP14/110 significantly ($p < 0.05$) decreased VEGFA expression (Fig. 5B), compared to control cells (HG), at all the tested concentrations. On the contrary, VP14/12 significantly decreased VEGFA expression ($p < 0.05$) only at the 10 μM concentration.

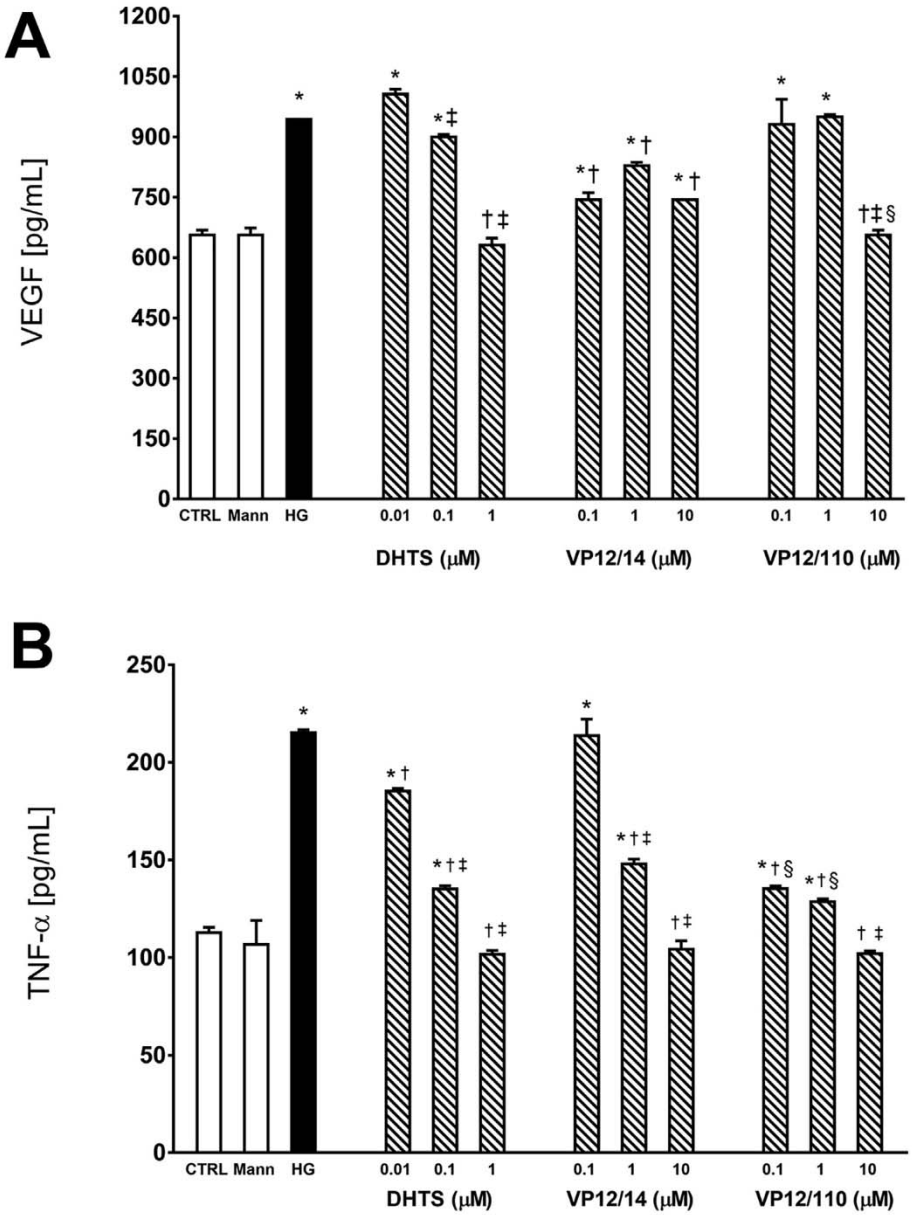

Fig. 5. VP12/14 and VP12/110 decrease VEGFA and TNFα release in an *in-vitro* model of diabetic retinopathy. VEGFA (A) and TNFα (B) protein HRECs released levels (pg/mL) were measured with ELISA kits. HRECs were exposed for 48 h to the osmotic control (mannitol; Mann) or high glucose levels (25 mM; HG), in the presence of different concentrations (0.01–1 μM) of DHTS, (0.1–10 μM) VP12/14 and VP12/110. Results are expressed as mean ± SD. One-way ANOVA and Tukey *post-hoc* test for multiple comparison were carried out. *$p < 0.05$ *vs*. CTRL or Mann; † $p < 0.05$ *vs.* HG; ‡ $p < 0.05$ *vs.* 0.01 μM DHTS, 0.1 μM VP12/14 or VP12/110 treatment; § $p < 0.05$ VP12/110 *vs.* VP12/14 (n = 4).

3.5. VP12/14 and VP12/110 decreased released protein levels of VEGF and TNFα in an in vitro model of diabetic retinopathy

We carried out measurement of the release by HRECs of VEGFA (pro-angiogenic growth factor) and TNFα (inflammatory cytokine) analyzing with commercial ELISA kits the medium of HRECs, challenged with high glucose levels (25 mM) and treated for 48 h with DHTS, VP12/14 and VP12/110. ELISA measurements are a completion of western blot analysis, since VEGFA and TNF-α mediate their biological function as paracrine factors. Human retinal endothelial cells, challenged with high glucose (HG, 25 mM) levels, released in the media significantly higher amounts of TNFα and VEGFα compared to control group (Fig. 5A, B). These findings agreed with western blotting analysis. Moreover, DHTS significantly ($p < 0.05$) decreased in a concentration-dependent manner both VEGFA and TNFα released protein levels in HRECs challenged with high glucose levels. VP12/14 significantly ($p < 0.05$) decreased VEGFA and TNFα levels compared to HG group, but a concentration-effect dependency was significantly ($p < 0.05$) observed only for TNFα. VP12/110 significantly ($p < 0.05$) decreased at 10 μM concentration VEGFA levels in medium of treated HRECs, to levels of control group and cell treated for 48 h with DHTS (1 μM). Moreover, V12/110 decreased TNFα release in a concentration-dependent manner similarly to DHTS, and likely inhibiting HuR/target mRNA interaction.

3.6. DHTS, VP12/14 and VP12/110 modulated VEGFA mRNA levels and exerted antiangiogenic activity

HRECs growth in high glucose (25 mM) media for 48 h expressed higher mRNA levels of VEGFA, compared to control cells, accordingly to previous reported data [4] (Fig. 6A). As reported above, we found that at DHTS, VP12/14 and VP12/110 significantly ($p < 0.05$) modulated HRECs protein expression (Fig. 4) and protein release of VEGFA and TNFα (Fig. 5). Furthermore, in order to prove the efficacy of tested compounds as anti-angiogenic small molecules, we tested the modulation of VEGFA expression (Fig. 6A, mRNA levels) in HRECs challenged with high glucose levels, along with tube-formation Matrigel assay (Fig. 6B,C,D), previously used for evaluation of angiogenesis potential of HRECs [35,36]. DHTS and VP compounds, tested at most effective concentration found in ELISA assays, significantly

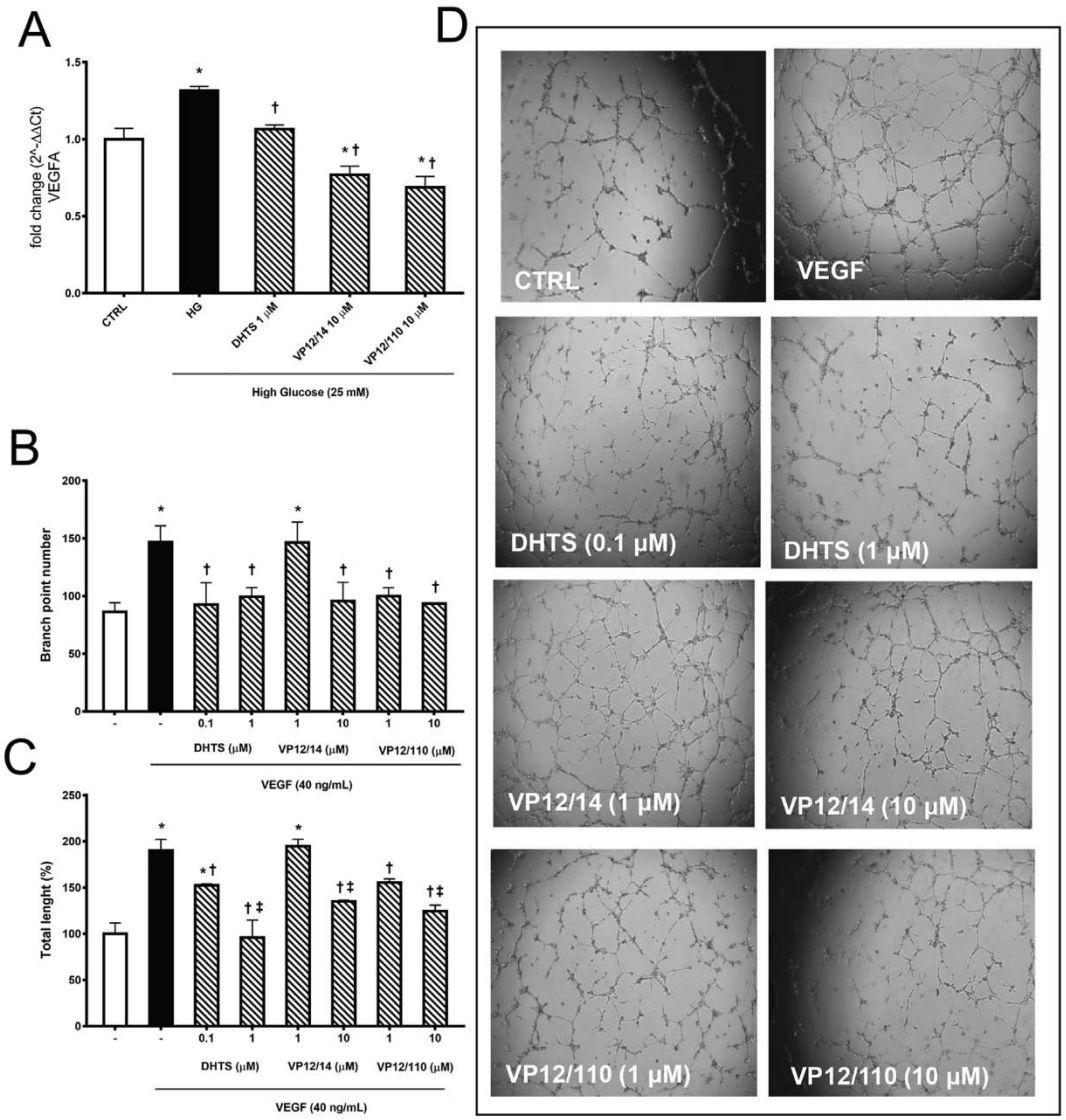

Fig. 6. DHTS, VP12/14 and VP12/110 decrease mRNA levels of VEGFA and exert antiangiogenic activity. A) Fold change of VEGFA mRNA levels normalized to 18S, in HRECs growth in control medium (5 mM glucose), high glucose medium (25 mM, HG) w/o DHTS (1 μM), VP12/14 (10 μM) and VP12/110 (10 μM). B) Tube-formation assay, number of branch points in HRECs. C) Tube-formation assay, tube length % of control. D) representative images of treatment groups: control, VEGFA (40 ng/ml) w/o DHTS (0.1–1 μM), VP12/14 (1–10 μM) and VP12/110 (1–10 μM). * $p < 0.05$ *vs.* control cells; † $p < 0.05$ *vs.* HG or VEGFA treatment group; ‡ < 0.05 *vs.* lowest tested concentration of DHTS, VP12/14 and VP12/110 (n = 4).

($p < 0.05$) decreased expression of VEGFA mRNA levels in HRECs challenged with high glucose (25 mM). Particularly, VP12/14 and VP12/110 decreased mRNA levels to values below control group (5 mM). These molecules likely destabilize mRNA levels of VEGFA and TNFα, accordingly to our hypothesis and as previously reported for DHTS [10]. Furthermore, DHTS and VP compounds significantly exerted an anti-angiogenic activity on HRECs treated with 40 ng/ml VEGFA in the tube-formation Matrigel assay (Fig. 6 B, C and D). DHTS, VP12/14 and VP12/110 significantly ($p < 0.05$) decreased number of branches point of new vessels (Fig. 6B). Additionally, all compounds decreased in a concentration-dependent manner ($p < 0.05$) the tube length of neo-vessels. According to ELISA data, VP12/14 was less effective in the tube-formation assay, then DHTS and VP12/110.

3.7. Molecular dynamics of VP12/14 and VP12/110 HuR complexes

After virtual screening, we carried out MMGBSA calculations to rescore screened ligands in order to guide the choice of hit compounds to be tested *in vitro*. Clustering analysis (SIFts ∩ MMGBSA $\Delta G_{coulomb}$ clustering) highlighted that only VP12/14 and VP12/110 clustered with active compounds. The predicted ΔG_{bind} of HuR (4EGL) bound to DHTS, VP12/14 and VP12/110 were −17.26 Kcal/mol, −6.00 Kcal/mol and −3.21 Kcal/mol, respectively. On the contrary MMGBSA calculations on 4ED5-inhibitor (HuR-mRNA-inhibitor) complexes predicted a $\Delta G_{binding}$ similar for DHTS (-65.71 Kcal/mol), VP12/14 (-70.25 Kcal/mol) and VP12/110 (-63.54 Kcal/mol) complexes. MMGBSA calculations approximate the ΔG_{bind} and, generally, those calculations correlate with *in vitro* activity. However, in the present *in vitro* study, the tested compounds showed an effectiveness ranking (DHTS≫VP12/110 > VP12/14) that did not correlate with either the predicted $\Delta G_{binding}$ of 4EGL-inhibitor complexes (DHTS≫VP12/14 > VP12/110) or of 4ED5-inhibitor complexes. Besides $\Delta G_{binding}$ calculations, we deeply analyzed the effects of HuR inhibitors at structural level by molecular dynamics simulation of HuR-inhibitor (compounds bound to 4EGL) and HuR-mRNA-inhibitor (compounds bound to 4ED5) complexes. Besides the binding mode similarity (SIFts clustering) of compounds at 4EGL (Fig. 7) and 4ED5 (Fig. 8) structures, analysis of molecular dynamics trajectories of each HuR-inhibitor and HuR-mRNA-

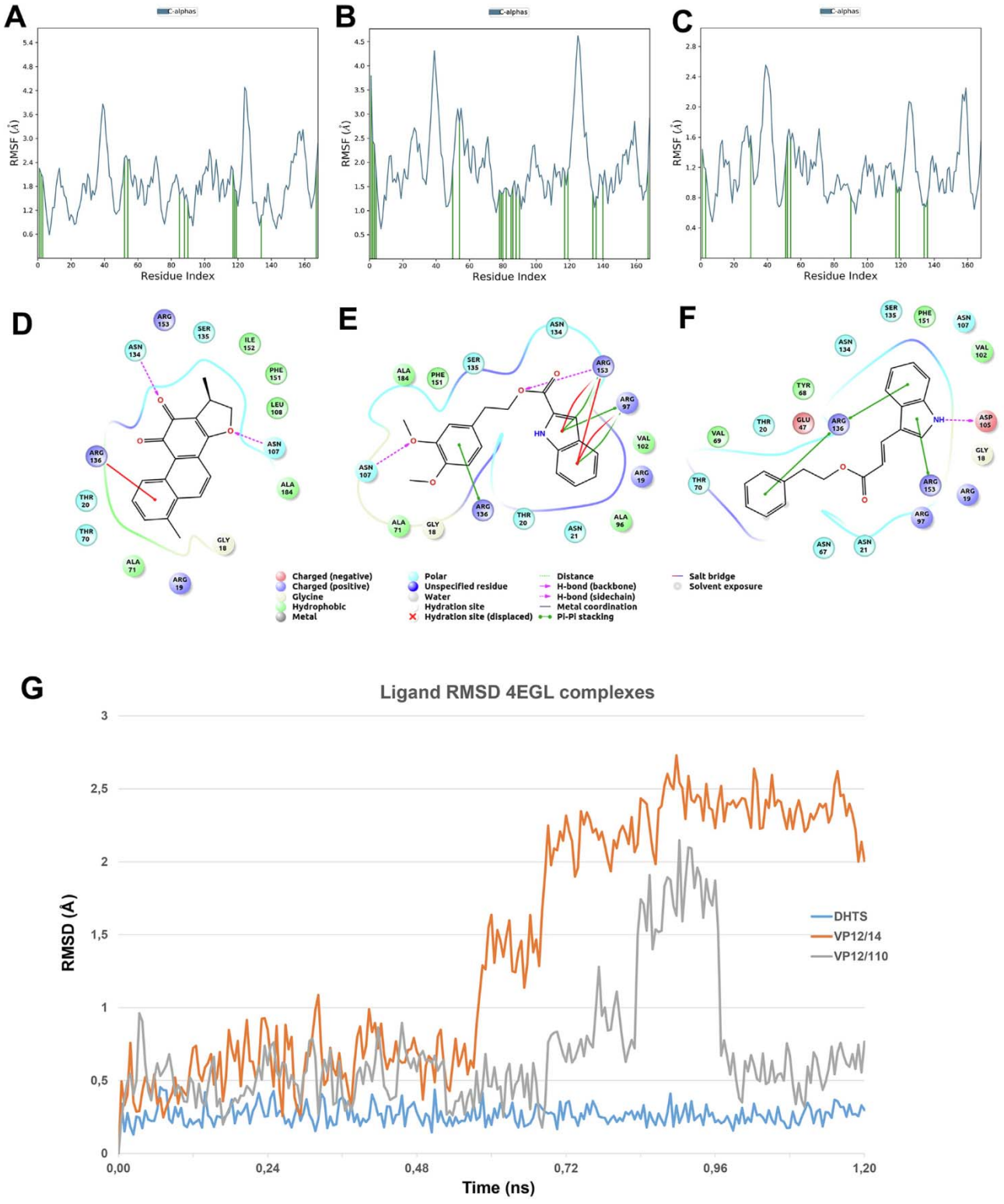

Fig. 7. Analysis of inhibitors/HuR complexes, 4EGL docking and molecular dynamics. (A) DHTS; (B) VP12/14 and (C) VP12/110 protein RMSF (blue line, Å) and ligand-protein contacts (green lines), in 4EGL complexes. (D) DHTS; (E) VP12/14 and (F) VP12/110 bidimensional protein-ligand contacts. (G) RMSD (Å) of ligands bound to HuR (PDB: 4EGL); blue line (DHTS), orange line (VP12/14), grey line (VP12/110). (For interpretation of the references to color in this figure legend, the reader is referred to the web version of this article.)

inhibitor complex revealed that DHTS, VP12/14 and VP12/110 modified protein and protein/mRNA dynamics with different mechanisms. Molecular dynamics analysis of HuR(4EGL)-inhibitor complexes revealed that VP12/110 significantly decreased HuR root mean square fluctuations (RMSF; max 2.6 Å – min 0.4 Å), compared to VP12/14 (RMSF; max 4.5 Å – min 0.5 Å) and DHTS (RMSF; max 4.2 Å – min 0.6 Å) (Fig. 7A, B, C). Moreover, VP12/110 decreased HuR RMSF despite fewer contacts with protein residues, compared to VP12/14 and DHTS (Fig. 7D, E, F). DHTS bound to HuR was characterized by a lower ligand root mean square deviation RMSD (0.264 ± 0.004 Å),

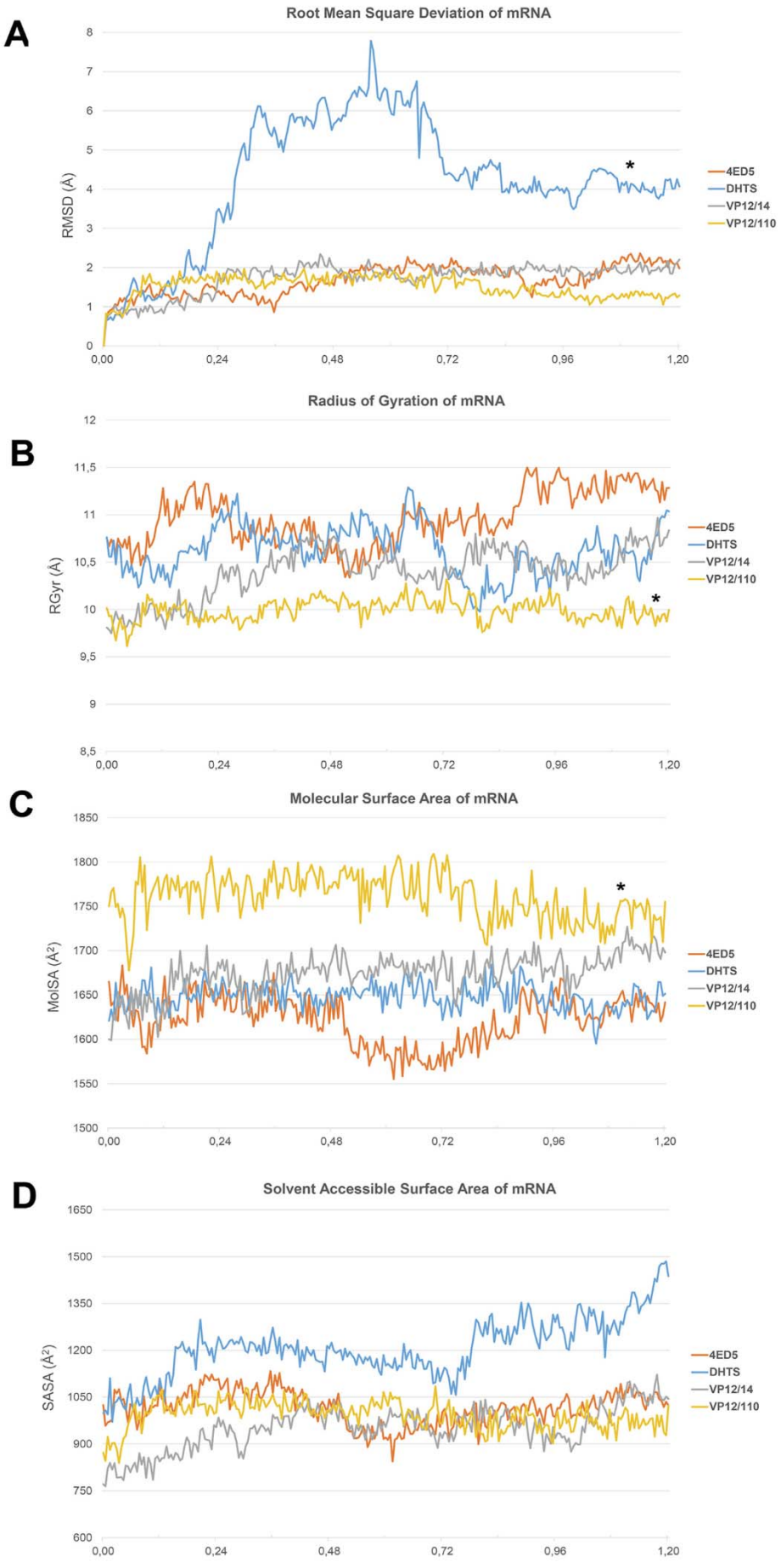

(caption on next page)

Fig. 8. Molecular dynamics analysis of inhibitors/HuR/mRNA complexes. A) RMSD of mRNA. B) Radius of gyration of mRNA. C) Molecular surface area of mRNA. D) Solvent accessible surface area of mRNA. *p < 0.05.

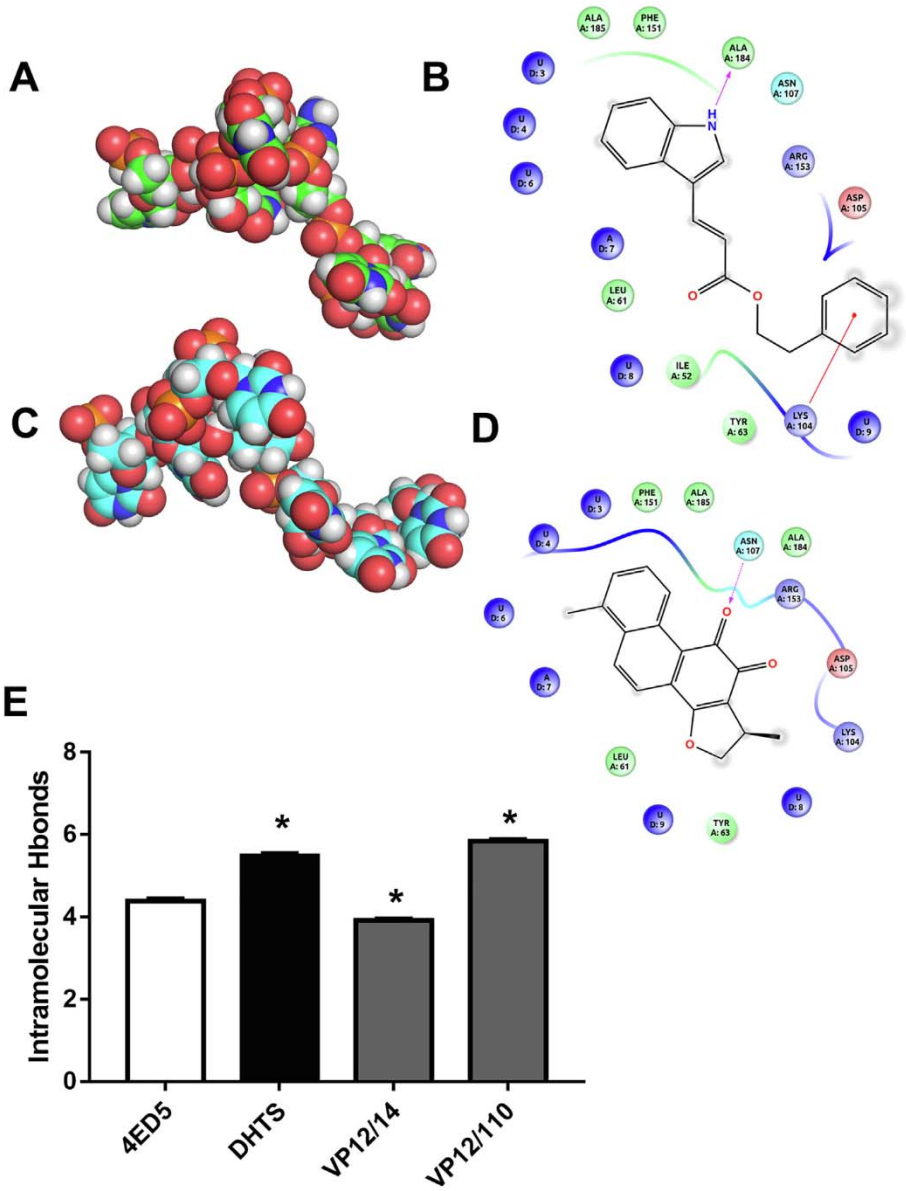

Fig. 9. Modification of the mRNA structure induced by VP12/110 and DHTS bound to the HuR-mRNA complex. A) Van der Walls (VdW) spheres representation of mRNA in the HuR-mRNA-VP12/110 complex (4ED5-inhibitor). B) 2D representation of VP12/110 bound to 4ED5. C) Van der Walls (VdW) spheres representation of mRNA in the HuR-mRNA-DHTS complex (4ED5-inhibitor). D) 2D representation of DHTS bound to 4ED5. E) Number of intramolecular Hbonds of mRNA in each analyzed complex, *p < 0.05 4ED5 *vs.* HuR-mRNA-inhibitor complexes.

compared to VP12/110 (0.69 ± 0.02 Å) and VP12/14 (1.40 ± 0.05 Å), meaning that DHTS showed less conformational fluctuation when bound to HuR (4EGL), compared to the other tested compounds. We also explored the capability of the tested compounds to interfere with HuR/mRNA complex (Fig. 8). Particularly, DHTS significantly ($p < 0.05$) increased the RMSD of mRNA bound to HuR, compared to VP12/14 and VP12/110 (Fig. 8A). While, VP12/110 significantly ($p < 0.05$) decreased the radius of gyration (Fig. 8B) and increased the molecular surface area (MolSA $Å^2$, Fig. 8C) of mRNA, compared to DHTS and VP12/14. In contrast to VP12/110, DHTS did not increase the molecular surface area (Van der Walls radius and steric hindrance), but increased the solvent accessible surface area of mRNA that likely undergoes to unfolding. On the basis of geometric considerations (radius of gyration, molecular surface area), VP12/110 modified the mRNA structure shape (cylinder > sphere) decreasing dimensions and increasing the steric hindrance of mRNA at HuR active cleft (Fig. 9A). On the contrary, DHTS unfolded the mRNA bound to HuR and changed mRNA conformation (increased RMSD compared to the structure at t0, along with solvent accessible surface area, Fig. 9C). Furthermore, DHTS and VP12/110 significantly and radically interfered with the mRNA conformation due to the formation of a greater number of intramolecular hydrogen bonds (Fig. 9E), compared to mRNA bound to HuR (4ED5) or in the complex 4ED5-VP12/14. Therefore, on the basis of molecular dynamics analysis, we can conclude that VP12/110 and DHTS could be able to inhibit HuR not only by competing with mRNA binding pocket of HuR, but also by modifying the mRNA structure in 4ED5, then inhibiting the function of HuR as an mRNA chaperone protein.

4. Discussion

VP12/14 and VP12/110, novel synthetized derivatives with an indole moiety, were identified through a virtual screening protocol as potential HuR inhibitors. Virtual screening was carried out by docking a focused set of 28 compounds at HuR (PDB:4EGL) and HuR-mRNA (PDB: 4ED5) structures (Figs. 1 and 2). The focused set was built by selecting ligands from a proprietary compound database containing 182 compounds, based on shared shape similarity with DHTS, a well characterized HuR inhibitor [10].

Docking results were rescored applying MMGBSA calculations and by clustering docked compounds with known active HuR inhibitors. Clustering was carried out by the intersection of Structural interaction fingerprints (SIFts) ∩ MMGBSA $\Delta G_{coulomb}$ calculated properties. Only two compounds, with indole moiety, of the screened dataset, possibly due to preliminary focusing on DHTS shape, clustered with the two active compounds DHTS and MS444. The preliminary shape similarity, using DHTS as template, was carried out to increase the success rate of virtual screening, because previous data report that DHTS mimics, bearing 7*a*-dihydro-1*H*-indole-4,5-dione moiety, showed higher efficacy than DHTS as inhibitors of HuR/mRNA complex formation [15]. After synthesis (Fig. 2C), we tested VP12/14 and VP12/110 in an *in vitro* model of diabetic retinopathy, along with DHTS, the well characterized HuR inhibitor [12]. Human retinal endothelial cells (HRECs) were treated for 24 and 48 h with (0.1–1-10–100 μM) DHTS, VP12/14 and VP12/110, w/o high glucose levels (25 mM), in order to test cell viability (MTT assay, Fig. 3). These compounds were generally well tolerated at the tested concentration by HRECs, grown in control (ctrl, 5 mM glucose) and high glucose media (HG, 25 mM glucose). However, DHTS showed the worst tolerability profile at 10 and 100 μM, at least in HRECs (ctrl and HG), compared to VP12/14 and VP12/110. While, VP12/110, at concentrations lower than 100 μM, showed a better tolerability profile than VP12/14 and DHTS. Thereafter, we explored the efficacy profile of the tested compounds in HRECs challenged with high glucose levels (HG, 25 mM) for 48 h. DHTS, VP12/14 and VP12/110 significantly decreased the expression of HuR, VEGF-A and TNFα (western blot analysis, Fig. 4) in HRECs exposed to HG, compared to untreated cells. Differences between DHTS, VP12/14 and VP12/110 efficacy profiles were found to be statistically significant ($p < 0.05$) in the assessment of VEGFA and TNFα levels released by HRECs after challenge with HG (25 mM glucose) (ELISA analysis, Fig. 5). The DHTS significantly decreased VEGFA and TNFα compared to HRECs exposed to HG. The DHTS effective concentration as HuR inhibitor was between 0.1 and 1 μM, accordingly to its IC_{50}, reported to be 0.149 ± 0.034 μM and 0.068 ± 0.016 nM in the electrophoresis mobility shift (REMSA) and AlphaScreen assays, respectively [10]. The comparison of VP12/14 and VP12/110 showed that VP12/110 was more effective than VP12/14 in decreasing the release of VEGF-A (10 μM) and TNFα (0.1–1 μM). Accordingly to the HuR chaperone function for mRNA of VEGFA [8,9,11,37] and TNFα[10], the our biochemical data suggested that VP12/14 and VP12/110 would act as HuR inhibitors, like DHTS [10], because decreased protein levels both in whole cell lysates and in medium of HRECs challenged with high glucose levels (25 mM). Furthermore, DHTS, VP12/14 and VP12/110 decreased VEGFA mRNA levels and exerted anti-angiogenic activity in HRECs stimulated with VEGFA (Fig. 6). Thus, to confirm our hypothesis, i.e. VP compounds share a mechanism of action similar to DHTS, a well characterized HuR inhibitor, we carried out time consuming *in silico* studies (MMGBSA and molecular dynamics) (Figs. 7–9).

The *in vitro* efficacy ranking of the tested compounds DHTS≫VP12/110 > VP12/14, correlated only partially with $\Delta G_{binding}$ calculated for HuR (4EGL)-inhibitor complexes DHTS≫VP12/14 > VP12/110. Therefore, we explored, through molecular dynamics simulations, alternative mechanism at HuR-mRNA-inhibitor complex. Molecular dynamics suggested, besides the binding mode similarity between DHTS and VP12/x derivatives, that tested compounds inhibited HuR at structural and molecular level with different mechanisms. Particularly, VP12/110 decreased the root mean square fluctuation (RMSF) of HuR (4EGL) to levels lower than DHTS and VP12/14. Moreover, DHTS and VP12/110 were more rigidly bound to HuR (4EGL) compared to VP12/14 (lower ligand root mean square deviation RMSD). The predicted $\Delta G_{binding}$ of DHTS, VP12/14 and VP12/110 in the 4ED5 complex (HuR-mRNA-inhibitor) was similar for all the tested compounds; but the analysis of mRNA dynamics showed significant differences between the three inhibitors-HuR-mRNA complexes (inhibitor-4ED5 analysis). Furthermore, DHTS increased the RMSD of the mRNA bound to HuR (4ED5 complex). Moreover, both DHTS and VP12/110 significantly increased the number of mRNA intramolecular hydrogen bonds, compared to mRNA bound to HuR or in the 4ED5- VP12/14 complex. Indeed, DHTS and VP12/110 significantly modified the structure of mRNA bound to HuR. Our data confirmed previous published results about DHTS binding in HuR active cleft and dynamics of DHTS-HuR (4EGL) complex [15]. Additionally, we found that DHTS and VP12/110 could be able not only to effectively bind HuR, competing with mRNA, but could also induce mRNA conformational changes in the HuR-mRNA complex, then interfering with the HuR function as an mRNA chaperone protein. ADME properties were predicted for compounds tested in the *in vitro* model of diabetic retinopathy. DHTS and VP12/14 were predicted to have a higher number of metabolites and reactive functional groups, which are predictive of potential *in vivo* toxicity. Moreover, the predicted ADME properties of DHTS and VP12/14 reflected the *in vitro* tolerability data. In fact, DHTS and VP12/14 showed a lower tolerability profile in HRECs (ctrl and HG groups), in comparison to VP12/110. All the tested compounds showed a predicted high score for human oral drug absorption. However, VP12/110 showed a lower score for CNS activity compared to DHTS and VP12/14 (i.e. probability to cross the blood brain barrier and blood retinal barrier). The present findings support the hypothesis that VP12/14 and VP12/110, are innovative molecules endowed with both anti-inflammatory and anti-angiogenic properties, likely working as disruptors of mRNA-HuR interaction. Other putative VP compounds-pharmacological target interactions could explain the VP12/14 and VP12/110 anti-angiogenic and anti-inflammatory activities, possibly interacting with other RNA binding proteins (RBPs), however the prediction/validation of a poly-pharmacological profile of these compounds is beyond the aim of this study. In particular, VP12/110, due to its interesting pharmacological profile and good *in vitro* tolerability, deserves further investigation, such as lead optimization. The present data suggested that VP12/110 represents a potential good candidate for DR treatment, and warrants further *in vivo* and clinical evaluation.

CRediT authorship contribution statement

Chiara Bianca Maria Platania: Investigation, Visualization, Validation, Formal analysis, Methodology, Conceptualization, Writing - original draft. **Valeria Pittalà:** Investigation, Visualization, Validation, Methodology, Conceptualization, Resources, Supervision, Project administration, Writing - review & editing. **Alessia Pascale:** Methodology, Conceptualization, Resources, Supervision, Project administration, Writing - review & editing. **Nicoletta Marchesi:** Investigation, Visualization, Validation. **Carmelina Daniela Anfuso:** Methodology, Conceptualization, Methodology, Conceptualization, Resources, Supervision, Project administration, Writing - review & editing. **Gabriella Lupo:** Methodology, Conceptualization, Resources, Supervision, Project administration, Writing - review & editing. **Martina Cristaldi:** Investigation, Visualization, Validation, Formal analysis. **Melania Olivieri:** Investigation, Visualization, Validation, Formal analysis. **Francesca Lazzara:** Investigation, Visualization, Validation. **Luisa Di Paola:** Investigation, Visualization, Validation, Resources, Supervision, Project administration. **Filippo Drago:** Writing - review & editing, Funding acquisition. **Claudio Bucolo:** Methodology, Conceptualization, Resources, Supervision, Project administration,

Writing - original draft, Writing - review & editing, Funding acquisition.

Declaration of Competing Interest

The authors declare that they have no known competing financial interests or personal relationships that could have appeared to influence the work reported in this paper.

Acknowledgements

This work was supported by National Grant PRIN 2015JXE7E8 from the Ministry of Education, University and Research (MIUR) and "Piano Triennale per la Ricerca – Linea Intervento 2, University of Catania, Italy".

References

[1] C. Bucolo, F. Drago, L.R. Lin, V.N. Reddy, Sigma receptor ligands protect human retinal cells against oxidative stress, NeuroReport (2006), https://doi.org/10.1097/01.wnr.0000199469.21734.e1.
[2] A.G. D'Amico, G. Maugeri, R. Reitano, C. Bucolo, S. Saccone, F. Drago, V. D'Agata, PACAP modulates expression of hypoxia-inducible factors in streptozotocin-induced diabetic rat retina, J. Mol. Neurosci. (2015), https://doi.org/10.1007/s12031-015-0621-7.
[3] G. Giurdanella, F. Lazzara, N. Caporarello, G. Lupo, C.D. Anfuso, C.M. Eandi, G.M. Leggio, F. Drago, C. Bucolo, S. Salomone, Sulodexide prevents activation of the PLA2/COX-2/VEGF inflammatory pathway in human retinal endothelial cells by blocking the effect of AGE/RAGE, Biochem. Pharmacol. 142 (2017) 145–154, https://doi.org/10.1016/j.bcp.2017.06.130.
[4] F. Lazzara, A. Fidilio, C.B.M. Platania, G. Giurdanella, S. Salomone, G.M. Leggio, V. Tarallo, V. Cicatiello, S. De Falco, C.M. Eandi, F. Drago, C. Bucolo, Aflibercept regulates retinal inflammation elicited by high glucose via the PlGF/ERK pathway, Biochem. Pharmacol. 168 (2019) 341–351, https://doi.org/10.1016/j.bcp.2019.07.021.
[5] P.P. Sfikakis, V. Grigoropoulos, I. Emfietzoglou, G. Theodossiadis, N. Tentolouris, E. Delicha, C. Katsiari, K. Alexiadou, E. Hatziagelaki, P.G. Theodossiadis, Infliximab for diabetic macular edema refractory to laser photocoagulation: a randomized, double-blind, placebo-controlled, crossover, 32-week study, Diabetes Care (2010), https://doi.org/10.2337/dc09-2372.
[6] M.T. Bolinger, D.A. Antonetti, Moving past anti-VEGF: Novel therapies for treating diabetic retinopathy, Int. J. Mol. Sci. (2016), https://doi.org/10.3390/ijms17091498.
[7] A. Pascale, S. Govoni, The complex world of post-transcriptional mechanisms: is their deregulation a common link for diseases? Focus on ELAV-like RNA-binding proteins, Cell. Mol. Life Sci. (2012), https://doi.org/10.1007/s00018-011-0810-7.
[8] M. Amadio, C. Bucolo, G.M. Leggio, F. Drago, S. Govoni, A. Pascale, The PKCβ/HuR/VEGF pathway in diabetic retinopathy, Biochem. Pharmacol. (2010), https://doi.org/10.1016/j.bcp.2010.06.033.
[9] M. Amadio, A. Pascale, S. Cupri, R. Pignatello, C. Osera, V. D'Agata, A.G. D'Amico, G.M. Leggio, B. Ruozi, S. Govoni, F. Drago, C. Bucolo, Nanosystems based on siRNA silencing HuR expression counteract diabetic retinopathy in rat, Pharmacol. Res. (2016), https://doi.org/10.1016/j.phrs.2016.07.042.
[10] V.G. D'Agostino, P. Lal, B. Mantelli, C. Tiedje, C. Zucal, N. Thongon, M. Gaestel, E. Latorre, L. Marinelli, P. Seneci, M. Amadio, A. Provenzani, Dihydrotanshinone-I interferes with the RNA-binding activity of HuR affecting its post-transcriptional function, Sci. Rep. (2015), https://doi.org/10.1038/srep16478.
[11] R. Nasti, D. Rossi, M. Amadio, A. Pascale, M.Y. Unver, A.K.H. Hirsch, S. Collina, Compounds interfering with Embryonic Lethal Abnormal Vision (ELAV) protein-RNA complexes: an avenue for discovering new drugs, J. Med. Chem. (2017), https://doi.org/10.1021/acs.jmedchem.6b01871.
[12] P. Lal, L. Cerofolini, V.G. D'Agostino, C. Zucal, C. Fuccio, I. Bonomo, E. Dassi, S. Giuntini, D. Di Maio, V. Vishwakarma, R. Preet, S.N. Williams, M.S. Fairlamb, R. Munk, E. Lehrmann, K. Abdelmohsen, S.R. Elezgarai, C. Luchinat, E. Novellino, A. Quattrone, E. Biasini, L. Manzoni, M. Gorospe, D.A. Dixon, P. Seneci, L. Marinelli, M. Fragai, A. Provenzani, Regulation of HuR structure and function by dihydrotanshinone-I, Nucleic Acids Res. (2017), https://doi.org/10.1093/nar/gkx623.
[13] Z. Wang, A. Bhattacharya, D.N. Ivanov, Identification of Small-Molecule Inhibitors of the HuR/RNA Interaction using a fluorescence polarization screening assay followed by NMR validation, PLoS ONE (2015), https://doi.org/10.1371/journal.pone.0138780.
[14] F. Vasile, S. Della Volpe, F.A. Ambrosio, G. Costa, M.Y. Unver, C. Zucal, D. Rossi, E. Martino, A. Provenzani, A.K.H. Hirsch, S. Alcaro, D. Potenza, S. Collina, Exploration of ligand binding modes towards the identification of compounds targeting HuR: a combined STD-NMR and Molecular Modelling approach, Sci. Rep. (2018), https://doi.org/10.1038/s41598-018-32084-z.
[15] L. Manzoni, C. Zucal, D. Di Maio, V.G. D'Agostino, N. Thongon, I. Bonomo, P. Lal, M. Miceli, V. Baj, M. Brambilla, L. Cerofolini, S. Elezgarai, E. Biasini, C. Luchinat, E. Novellino, M. Fragai, L. Marinelli, A. Provenzani, P. Seneci, Interfering with HuR-RNA interaction: design, synthesis and biological characterization of tanshinone mimics as novel, effective HuR inhibitors, J. Med. Chem. (2018), https://doi.org/10.1021/acs.jmedchem.7b01176.
[16] S. Della Volpe, R. Nasti, M. Queirolo, M.Y. Unver, V.K. Jumde, A. Dömling, F. Vasile, D. Potenza, F.A. Ambrosio, G. Costa, S. Alcaro, C. Zucal, A. Provenzani, M. Di Giacomo, D. Rossi, A.K.H. Hirsch, S. Collina, Novel compounds targeting the RNA-binding protein HuR. Structure-based design, synthesis, and interaction studies, ACS Med. Chem. Lett. (2019), https://doi.org/10.1021/acsmedchemlett.8b00600.
[17] H. Wang, F. Zeng, Q. Liu, H. Liu, Z. Liu, L. Niu, M. Teng, X. Li, The structure of the ARE-binding domains of Hu antigen R (HuR) undergoes conformational changes during RNA binding, Acta Crystallogr. D Biol. Crystallogr. (2013), https://doi.org/10.1107/S0907444912047828.
[18] A. del Sol, M.J. Araúzo-Bravo, D. Amoros, R. Nussinov, Modular architecture of protein structures and allosteric communications: potential implications for signaling proteins and regulatory linkages, Genome Biol. (2007), https://doi.org/10.1186/gb-2007-8-5-r92.
[19] S. Cimini, L. Di Paola, A. Giuliani, A. Ridolfi, L. De Gara, GH32 family activity: a topological approach through protein contact networks, Plant Mol. Biol. 92 (2016) 401–410, https://doi.org/10.1007/s11103-016-0515-2.
[20] C.B.M. Platania, L. Di Paola, G.M. Leggio, G.L. Romano, F. Drago, S. Salomone, C. Bucolo, Molecular features of interaction between VEGFA and anti-angiogenic drugs used in retinal diseases: a computational approach, Front. Pharmacol. 6 (2015) 248, https://doi.org/10.3389/fphar.2015.00248.
[21] S. Tasdighian, L. Di Paola, M. De Ruvo, P. Paci, D. Santoni, P. Palumbo, G. Mei, A. Di Venere, A. Giuliani, Modules identification in protein structures: the topological and geometrical solutions, J. Chem. Inf. Model. (2014), https://doi.org/10.1021/ci400218v.
[22] L. Di Paola, C.B.M. Platania, G. Oliva, R. Setola, F. Pascucci, A. Giuliani, Characterization of protein-protein interfaces through a protein contact network approach, Front. Bioeng. Biotechnol. 3 (2015) 170, https://doi.org/10.3389/fbioe.2015.00170.
[23] C.B.M. Platania, G. Giurdanella, L. Di Paola, G.M. Leggio, F. Drago, S. Salomone, C. Bucolo, P2X7 receptor antagonism: implications in diabetic retinopathy, Biochem. Pharmacol. (2017), https://doi.org/10.1016/j.bcp.2017.05.001.
[24] L. Di Paola, A. Giuliani, Protein contact network topology: a natural language for allostery, Curr. Opin. Struct. Biol. 31 (2015) 43–48, https://doi.org/10.1016/j.sbi.2015.03.001.
[25] N.C. Meisner, M. Hintersteiner, K. Mueller, R. Bauer, J.M. Seifert, H.U. Naegeli, J. Ottl, L. Oberer, C. Guenat, S. Moss, N. Harrer, M. Woisetschlaeger, C. Buehler, V. Uhl, M. Auer, Identification and mechanistic characterization of low-molecular-weight inhibitors for HuR, Nat. Chem. Biol. (2007), https://doi.org/10.1038/nchembio.2007.14.
[26] M.-J. Chae, H.Y. Sung, E.-H. Kim, M. Lee, H. Kwak, C.H. Chae, S. Kim, W.-Y. Park, Chemical inhibitors destabilize HuR binding to the AU-rich element of TNF-alpha mRNA, Exp. Mol. Med. 41 (2009) 824–831, https://doi.org/10.3858/emm.2009.41.11.088.
[27] V. Pittala, L. Vanella, L. Salerno, C. Di Giacomo, R. Acquaviva, M. Raffaele, G. Romeo, M.N. Modica, O. Prezzavento, V. Sorrenti, Novel Caffeic Acid Phenethyl Ester (Cape) analogues as inducers of heme oxygenase-1, Curr. Pharm. Des. (2017), https://doi.org/10.2174/1381612823666170210151411.
[28] V. Pittalà, L. Salerno, G. Romeo, M.A. Siracusa, M.N. Modica, G.L. Romano, S. Salomone, F. Drago, C. Bucolo, Effects of novel hybrids of caffeic acid phenethyl ester and NSAIDs on experimental ocular inflammation, Eur. J. Pharmacol. (2015), https://doi.org/10.1016/j.ejphar.2015.02.012.
[29] V. Pittala, A. Fidilio, F. Lazzara, C.B.M. Platania, L. Salerno, R. Foresti, F. Drago, C. Bucolo, Effects of novel nitric oxide-releasing molecules against oxidative stress on retinal pigmented epithelial cells, Oxid. Med. Cell. Longevity 2017 (2017) 1420892, https://doi.org/10.1155/2017/1420892.
[30] G. Romeo, L. Materia, V. Pittalà, M. Modica, L. Salerno, M. Siracusa, F. Russo, K.P. Minneman, New 1,2,3,9-tetrahydro-4H-carbazol-4-one derivatives: analogues of HEAT as ligands for the α1-adrenergic receptor subtypes, Bioorg. Med. Chem. (2006), https://doi.org/10.1016/j.bmc.2006.04.002.
[31] V. Pittala, M.A. Siracusa, M.N. Modica, L. Salerno, A. Pedretti, G. Vistoli, A. Cagnotto, T. Mennini, G. Romeo, Synthesis and molecular modeling of 1H-pyrrolopyrimidine-2,4-dione derivatives as ligands for the alpha1-adrenoceptors, Bioorg. Med. Chem. 19 (2011) 5260–5276, https://doi.org/10.1016/j.bmc.2011.06.043.
[32] L. Salerno, V. Pittala, M.N. Modica, M.A. Siracusa, S. Intagliata, A. Cagnotto, M. Salmona, R. Kurczab, A.J. Bojarski, G. Romeo, Structure-activity relationships and molecular modeling studies of novel arylpiperazinylalkyl 2-benzoxazolones and 2-benzothiazolones as 5-HT(7) and 5-HT(1A) receptor ligands, Eur. J. Med. Chem. 85 (2014) 716–726, https://doi.org/10.1016/j.ejmech.2014.08.023.
[33] V. Pittalà, L. Vanella, C.B. Maria Platania, L. Salerno, M. Raffaele, E. Amata, A. Marrazzo, G. Floresta, G. Romeo, K. Greish, S. Intagliata, C. Bucolo, V. Sorrenti, Synthesis, in vitro and in silico studies of HO-1 inducers and lung antifibrotic agents, Future, Med. Chem. (2019), https://doi.org/10.4155/fmc-2018-0448.
[34] C.T. Rueden, J. Schindelin, M.C. Hiner, B.E. DeZonia, A.E. Walter, E.T. Arena, K.W. Eliceiri, Image J2: ImageJ for the next generation of scientific image data, BMC Bioinf. (2017), https://doi.org/10.1186/s12859-017-1934-z.
[35] U.C.S. Yadav, S.K. Srivastava, K.V. Ramana, Prevention of VEGF-induced growth and tube formation in human retinal endothelial cells by aldose reductase inhibition, J. Diab. Complications (2012), https://doi.org/10.1016/j.jdiacomp.2012.04.017.
[36] G. Giurdanella, F. Lazzara, N. Caporarello, G. Lupo, C.D. Anfuso, C.M. Eandi, G.M. Leggio, F. Drago, C. Bucolo, S. Salomone, Sulodexide prevents activation of the PLA2/COX-2/VEGF inflammatory pathway in human retinal endothelial cells by blocking the effect of AGE/RAGE, Biochem. Pharmacol. (2017), https://doi.org/10.1016/j.bcp.2017.06.130.
[37] C.D. Anfuso, G. Lupo, L. Romeo, G. Giurdanella, C. Motta, A. Pascale, C. Tirolo, B. Marchetti, M. Alberghina, Endothelial cell-pericyte cocultures induce PLA $_2$ protein expression through activation of PKCα and the MAPK/ERK cascade, J. Lipid Res. (2007), https://doi.org/10.1194/jlr.M600489-JLR200.